Developmental Biology 478 (2021) 89–101

Contents lists available at ScienceDirect

Developmental Biology

journal homepage: www.elsevier.com/locate/developmentalbiology

IMPDH forms the cytoophidium in zebrafish

Gerson Dierley Keppeke [a,d,1], Chia-Chun Chang [a,1], Christopher L. Antos [a], Min Peng [b], Li-Ying Sung [b,c], Luis Eduardo Coelho Andrade [d], Ji-Long Liu [a,*]

[a] School of Life Science and Technology, ShanghaiTech University, Shanghai, 201210, China
[b] Institute of Biotechnology, National Taiwan University, Taipei, 106, Taiwan
[c] Agricultural Biotechnology Research Center, Academia Sinica, Taipei, 115, Taiwan
[d] Rheumatology Division, Escola Paulista de Medicina, Universidade Federal de Sao Paulo, Sao Paulo, SP, 04023-062, Brazil

ARTICLE INFO

Keywords:
IMPDH
Cytoophidium
Larval zebrafish
Adult zebrafish

ABSTRACT

Inosine monophosphate dehydrogenase (IMPDH) catalyzes the rate-limiting step in *de novo* guanine nucleotide biosynthesis. Its activity is negatively regulated by the binding of GTP. IMPDH can form a membraneless subcellular structure termed the cytoophidium in response to certain changes in the metabolic status of the cell. The polymeric form of IMPDH, which is the subunit of the cytoophidium, has been shown to be more resistant to the inhibition by GTP at physiological concentrations, implying a functional correlation between cytoophidium formation and the upregulation of GTP biosynthesis. Herein we demonstrate that zebrafish IMPDH1b and IMPDH2 isoforms can assemble abundant cytoophidium in most of cultured cells under stimuli, while zebrafish IMPDH1a shows distinctive properties of forming the cytoophidium in different cell types. Point mutations that disrupt cytoophidium structure in mammalian models also prevent the aggregation of zebrafish IMPDHs. In addition, we discover the presence of the IMPDH cytoophidium in various tissues of larval and adult fish under normal growth conditions. Our results reveal that polymerization and cytoophidium assembly of IMPDH can be a regulatory machinery conserved among vertebrates, and with specific physiological purposes.

1. Introduction

Macromolecules that assemble into membraneless organelles are a common feature of different forms of life. These subcellular structures, such as ribosomes, cytoplasmic processing bodies (P bodies), uridine-rich small nuclear ribonucleoprotein bodies (U bodies), glycine/tryptophan bodies (GW bodies), proteasomes and purinosomes, have been getting increasing attention recently (Liu, 2016).

Over the last 10 years, many groups have intensively worked on a kind of membraneless structure termed the cytoophidium ("cellular snake" in Greek, cytoophidia in plural) in a variety of model organisms. In mammalian cells, the cytoophidium appears filamentous with length ranging from hundreds of nanometers up to longer than 10 μm, or in donut-like circular forms with a wide size range. Accordingly, these structures have been named "rods and rings" (RR) by some groups. The cytoophidium was first reported to be comprised of cytidine triphosphate synthase (CTPS), and then inosine 5′-monophosphate dehydrogenase (IMPDH) was also identified to have the cytoophidium-forming property in mammalian models (Carcamo et al., 2011; Liu, 2010). IMPDH and CTPS cytoophidia are substantially distinct structures yet frequently aligned side-by-side with each other in the cell (Chang et al., 2018). We have recently found that both IMPDH and CTPS form cytoophidia in mouse developmental thymocytes (Peng et al., 2021). To date, dozens of metabolic enzymes have been demonstrated to assemble into filamentous or dot-like aggregates through a genome-wide screening in budding yeast, suggesting that forming large complexes could be a common regulatory mechanism of metabolic enzymes (Lynch et al., 2020; Noree et al., 2019; Shen et al., 2016).

IMPDH contains two domains, a catalytic domain and a Bateman domain. While the catalytic domain processes the rate-limiting step of *de novo* guanine nucleotide synthesis, in which IMP is converted into XMP in a NAD^+-dependent manner, the Bateman domain serves for allosteric modulation of its activity. Binding of GDP/GTP at the Bateman domain reduces affinity to its substrate IMP, while binding of ATP promotes enzyme activity (Buey et al., 2015; Hedstrom, 2009). Human IMPDH (hIMPDH) forms octamers spontaneously in vitro. In the presence of ATP,

* Corresponding author.
E-mail address: liujl3@shanghaitech.edu.cn (J.-L. Liu).
[1] These authors contributed equally to this work.

https://doi.org/10.1016/j.ydbio.2021.05.017
Received 20 September 2020; Received in revised form 17 May 2021; Accepted 18 May 2021
Available online 25 May 2021
0012-1606/© 2021 Elsevier Inc. All rights reserved.

IMDPH octamers can pile up to form a polymeric structure, which would be further stabilized by IMP and destabilized by the binding of GTP (Johnson and Kollman, 2020; Juda et al., 2014; Lin et al., 2018). The cytoophidium is formed by a large bundle of IMPDH polymers. It has been shown that IMPDH is much less sensitive to its negative regulator GTP in the polymeric state. Since IMPDH plays a pivotal role in regulating the production of guanine nucleotides in the cell, massive polymerization of IMPDH may facilitate the accumulation of GDP/GTP in cells. This could be particularly important to those cells with a higher demand for nucleotides such as highly proliferative cells (Fernandez--Justel et al., 2019; Johnson and Kollman, 2020).

The IMPDH cytoophidium was first observed in cells under treatment with an IMPDH inhibitor, mycophenolic acid (MPA) (Ji et al., 2006). Thereafter, many other conditions have been shown to promote IMPDH cytoophidium assembly, such as glutamine deficiency, disturbance of one-carbon pathway and treatment by a variety of clinical drugs. These findings imply that cytoophidium formation is correlated with changes in the metabolic state of the cell (Calise et al., 2014, 2016; Keppeke et al., 2016). Yet, the IMPDH cytoophidium is also observed in certain cells and tissues without additional stimulus, such as mouse pluripotent stem cells, antigen-activated T lymphocytes, retinal photoreceptor cells, and some tumors, including acral melanomas and clear cell renal cell carcinoma (Calise et al., 2018; Duong-Ly et al., 2018; Keppeke et al., 2018, 2020; Plana-Bonamaiso et al., 2020; Ruan et al., 2020).

Because of its essential role in *de novo* guanine nucleotide production, IMPDH has been considered as a promising candidate for immunosuppressant, antiviral and anticancer drugs for decades (Hedstrom, 2009; Naffouje et al., 2019). However, little is known about the physiological importance of IMPDH cytoophidium. Herein, we provide evidences to demonstrate that, among three zebrafish IMPDH (zfIMPDH) isoforms, zfIMPDH1b and zfIMPDH2 can form abundant cytoophidia in cells under certain conditions, while zfIMPDH1a shows distinctive tendency to form the cytoophidium in different cell types. We also apply mutagenesis to disrupt zfIMPDH polymerization, suggesting a structural similarity between polymers of zfIMPDH and hIMPDH. Immunofluorescence indicates that zfIMPDH cytoophidia appear naturally in multiple tissues of zebrafish at different developmental stages. Our findings reinforce the theory that the IMPDH cytoophidium is a common feature of vertebrate IMPDH, and indicate that zebrafish is a suitable model for further research on the physiological functions of this structure.

2. Results

2.1. zfIMPDH isoforms exhibit different propensity to form cytoophidia

While the CTPS polymer structure has been revealed in various organisms across prokaryotes and eukaryotes, research on the IMPDH polymer and cytoophidium is still limited to mammalian models. We aligned IMPDH2 sequences of some representative vertebrates, and the result shows 78% sequence identity among them (Supplementary Fig. 1). Sequences of human and mouse (mammals), chicken (bird), Eastern coral snake (reptile), African clawed frog (amphibian) and zebrafish (bony fish) IMPDH2 all have 514 amino acids, while the ghost shark (cartilaginous fish) IMPDH2 has 538 amino acids with an additional exon. The sequence similarity reaches 81.7% without the extra exon, indicating the high degree of conservation of IMPDH sequences among vertebrates. Therefore, we wondered whether the polymerization and cytoophidium-forming properties of IMPDH are conserved in non-mammal vertebrates.

Zebrafish has three IMPDH isoforms, 1a, 1b and 2, encoded by distinct genes. We compared the sequences of all three isoforms with the human IMPDH1 and IMPDH2, and observed that both zfIMPDH1a and 1b are similar to hIMPDH1 with 85.5% and 90.7% sequence identity, respectively, while zfIMPDH2 is similar to hIMPDH2 with 91.4% sequence identity (Fig. 1A and B).

In mammals, IMPDH1 is expressed at low levels in most tissues except for the retina, where it is highly expressed, while IMPDH2 is the predominant isoform in most tissues and is upregulated in proliferative cells (Carr et al., 1993; Hager et al., 1995; Senda and Natsumeda, 1994). We analyzed mRNA expression levels of zfIMPDH isoforms in various tissues. Interestingly, zfIMPDH1a was almost exclusively expressed in the eye, at

A

Sequence identity (%)

	zfIMPDH1a	zfIMPDH1b	zfIMPDH2	hIMPDH1
zfIMPDH1b	88.4			
zfIMPDH2	78.7	83.1		
hIMPDH1	85.5	90.7	81.9	
hIMPDH2	80.3	85.0	91.4	84.0

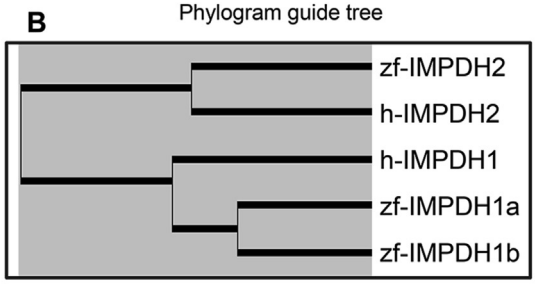

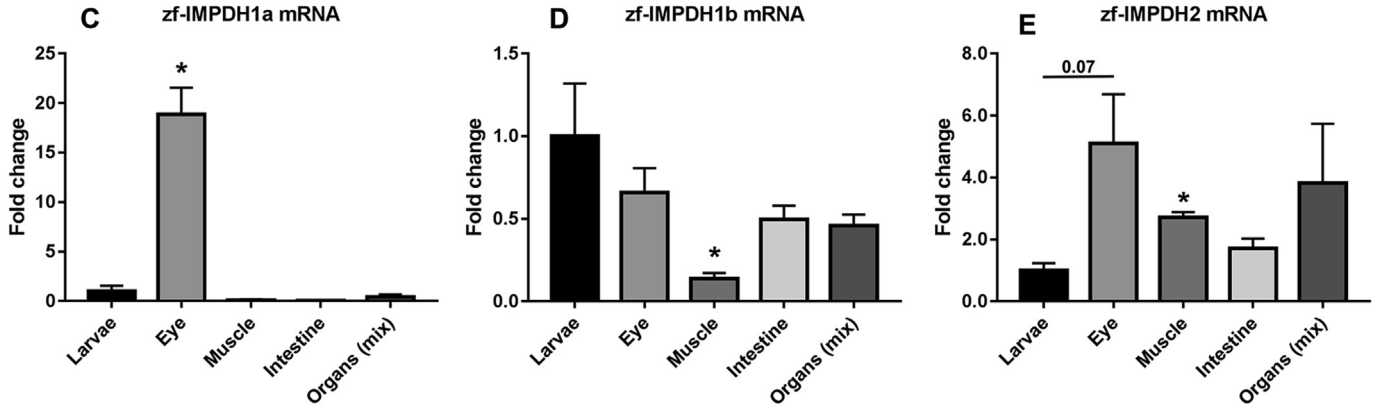

Fig. 1. Differential expression patterns of three zfIMPDH isoforms. (A) Protein sequence comparison between human and zebrafish IMPDH isoforms. (B) Phylogram guide for human and zebrafish IMPDH sequences. (C–E) Relative mRNA levels of zfIMPDH isoforms in different tissues. n = 4 adult specimens and n = 2 larval specimens (10 dpf). Larval Ct average was considered as 1. (Error bars = S.E.M. $^*p < 0.05$, *t*-test).

about 20-fold higher than the levels in other tissues (Fig. 1C). zfIMPDH1b showed the highest expression levels in the larval stage, with about twice the level of adult eyes, intestine and a mix of organs, and 7-fold the level of muscle (Fig. 1D). On the other hand, zfIMPDH2 mRNA shows generally higher levels in adult tissues than larvae, although the difference is only statistically significant between larvae and adult muscle (Fig. 1E). These data are consistent with a previous study by (Li et al., 2015) which reports about 1.5 times increased expression level of zfIMPDH1a in the eye, despite our results suggest a much higher relative expression level. The expression patterns of the zfIMPDH1b and zfIMPDH2 are also generally consistent between these two studies.

In order to determine the cytoophidium-forming properties of each zfIMPDH isoform, we cloned the isoforms into constructs and expressed them in HeLa cells. In the condition without additional stimulus, zfIMPDH1b assembles into the cytoophidium spontaneously in 40% of cells, while zfIMPDH1a and zfIMPDH2 appear in a diffused pattern.

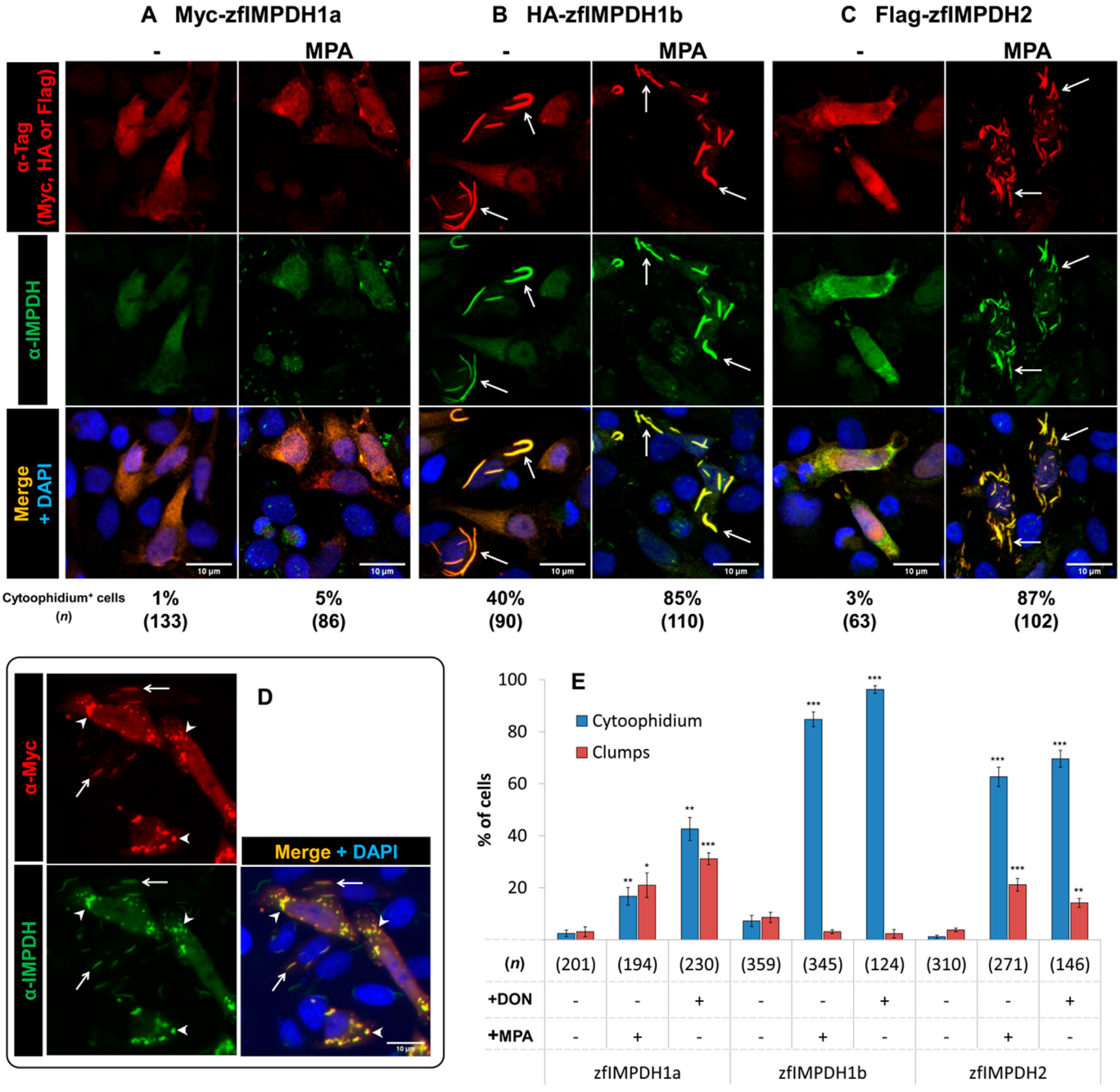

Fig. 2. Diverse zfIMPDHs cytoophidium-forming properties *in vitro*. (A–C) zfIMPDH isoforms were cloned with N-terminal tags and expressed in HeLa cells. Immunofluorescence probing on transfected HeLa cells under conditions with or without treatment of MPA (100 μM for 2 h). Myc-tag, HA-tag and Flag-tag are shown in red and antibody against IMPDH is shown in green. Cytoophidia formed by zfIMPDH are indicated by arrows in B and C. The proportion of cells with cytoophidia and the number of cells were counted (*n*) is shown below each panel. (D) HEp-2 cells expressing zfIMPDH1a were treated with DON (100 μM for 2 h) before fixation. Cytoophidia and clumps that contain zfIMPDH1a are indicated by arrows and arrowheads, respectively. Scale bars = 10 μm. (E) Bar graph showing the quantification of the proportion of zfIMPDH expressing HEp-2 cells with cytoophidia or clumps. Only transfected cells were counted and the number of cells counted in each group is shown as (*n*). (Error bars = S.E.M. *p < 0.05; **p < 0.01; ***p < 0.001, proportions were compared by *t*-test with the respective isoform without treatment.) In all groups with MPA treatment, endogenous cytoophidia in non-transfected cells are labeled by the α-IMPDH antibody.

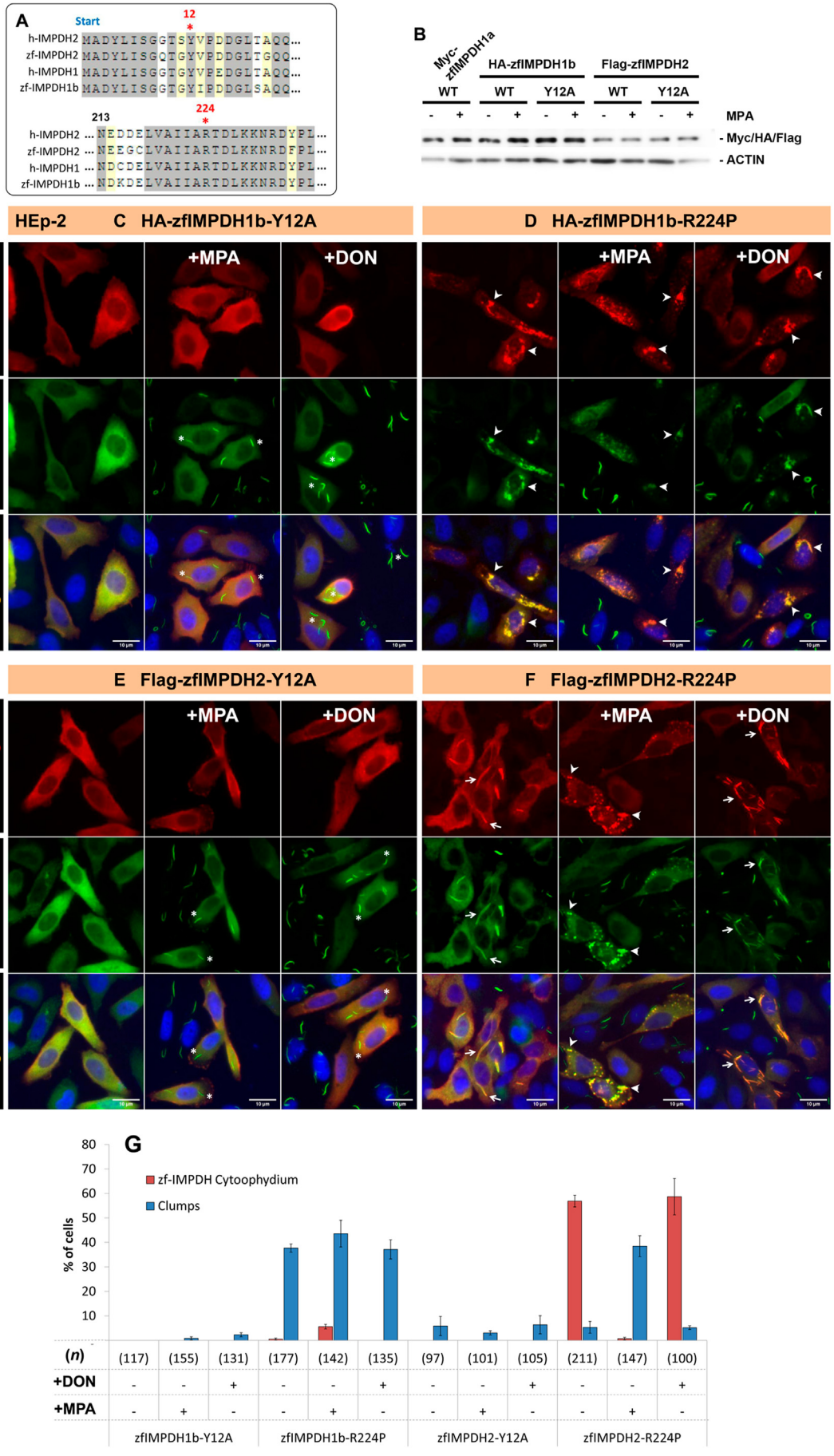

(caption on next page)

Fig. 3. Disruption of zfIMPDHs cytoophidium-forming properties with point mutations. (A) Sequence comparison of human and zebrafish IMPDH isoforms at regions around Lys12 and Arg224. (B) Immunoblotting of HeLa cells expressing WT or Y12A mutant zfIMPDH isoforms under conditions with or without MPA treatments shows similar expression levels of WT and Y12A mutant zfIMPDHs. (C–F) Immunofluorescence of HEp-2 cells expressing Y12A or R224P mutant zfIMPDH1b and zfIMPDH2. Cells were treated with MPA or DON for 2 h before fixation. Asterisks in panels C and E indicates the cells with endogenous cytoophidia, but not the zf-IMPDH cytoophidium. Arrows and arrowheads in panels D and F indicate zfIMPDH cytoophidia and clumps, respectively. Scale bars = 10 μm. (G) Quantification of the proportion of HEp-2 cells with zfIMPDH cytoophidia or clumps under the conditions shown in (C–F). Only transfected cells were counted and the number of cells counted (*n*) is shown for each group. Error bars = S.E.M. With MPA and DON treatments, non-transfected cells also present endogenous cytoophidia, which are labeled by the α-IMPDH antibody.

Intriguingly, upon treatment with the IMPDH inhibitor MPA, which induced abundant cytoophidia in ≥85% of cells expressing zfIMPDH1b and zfIMPDH2, only few cytoophidia were observed in about 5% of zfIMPDH1a-transfected HeLa cells (Fig. 2A–C). The sequences of zfIMPDH1a and zfIMPDH1b are 88.4% identical, although an extra exon is only present at the C-terminus of zfIMPDH1a (Fig. 1A). We sought to elucidate if this additional 30 a.a. long peptide could affect the filament-forming property of zfIMPDH1a. Thus, we removed the C-terminus of zfIMPDH1a by introducing a stop codon at the position of residue 510. However, zfIMPDH1a$^{\Delta 510\text{-}544}$ did not form the cytoophidium in HeLa cells even upon MPA treatment (Supplementary Figure 3D), indicating that the difference between zfIMPDH1a and 1b at the C-terminus does not explain their distinct filament-forming properties.

We further investigated the cytoophidium-forming properties of individual zfIMPDH isoforms in different cell lines and conditions. In HEp-2 cells treated with 6-diazo-5-oxo-L-norleucine (DON), a glutamine analog that can induce IMPDH cytoophidium assembly (Carcamo et al., 2011), zfIMPDH1a is present in cytoophidia in ~40% of cells and aggregates in sphere or in an irregular shape (clumps) in ~30% of cells (Fig. 2D). Although given clumps do not appear in a filamentous structure, we could not exclude the possibility that they are also formed by IMPDH polymers. Different from the HeLa cells, zfIMPDH1b assembled spontaneous cytoophidium in only 7% of HEp-2 cells. Upon MPA or DON treatment, zfIMPDH1b and zfIMPDH2 isoforms assembled into cytoophidia in ≥85% and ≥63% of cells, respectively (Fig. 2E and Supplementary Figure 2). Altogether, these data show that zfIMPDH isoforms display distinctive cytoophidium-forming tendencies.

2.2. Point mutations impede zfIMPDH cytoophidium assembly

Previous structural studies have shown that a single point mutation could result in remarkable changes in cytoophidium formation. For instance, the Y12A mutation on hIMPDH2 disrupts polymerization, while the R224P mutation results in irreversible aggregation of hIMPDH1 and no-cytoophidium pattern of hIMPDH2 (Anthony et al., 2017; Fernandez-Justel et al., 2019; Keppeke et al., 2018). These two critical positions are conserved in most vertebrate IMPDHs, including all zfIMPDH isoforms (Fig. 3A and Supplementary Figure 1). To test if Y12A and R224P mutations could have similar effects on zfIMPDH1b and 2, we introduced the point mutations into both isoforms, and treated HEp-2 and HeLa cells with MPA or DON after transfection. As the result, Y12A completely prevented assembly of the cytoophidium of both isoforms in both HEp-2 and HeLa cells with no significant changes in the expression levels (Fig. 3B, C, E and G, and Supplementary Figs. 3A and B, respectively). Meanwhile, zfIMPDH1b-R224P could not assemble the cytoophidium in HEp-2 and HeLa cells, but spontaneously formed irregular clumps in ~40% of cells (arrowheads in Fig. 3D). This proportion of cells with clumps was not changed when cells were further treated with MPA or DON (Fig. 3G and Supplementary Fig. 3C). On the other hand, zfIMPDH2-R224P spontaneously assembled the cytoophidium in ~50% of HEp-2 cells, and a similar proportion was observed with DON treatment (Fig. 3G). However, under MPA treatment all the cytoophidium turned into clumps in ~40% of the cells (Fig. 3F and G).

Y12A point mutation abrogates cytoophidium in zfIMPDH1b and 2. However, in ~50% of transfected HEp-2 cells under MPA or DON treatment (asterisks in Fig. 3C and E), cytoophidia formed by endogenous hIMPDH, which were not labeled by anti-HA and anti-Flag antibodies, were observed, suggesting that zfIMPDHs do not interact with hIMPDH, or octamers containing both human and mutant zfIMPDHs are excluded from polymers. We have previously demonstrated that human IMPDH1 and IMPDH2 always locate within the same cytoophidium structures (Keppeke et al., 2018). Thus, to test if different zfIMPDH isoforms assemble the same filaments, we co-transfected cells with constructs encoding zfIMPDH1b and zfIMPDH2 with or without Y12A point-mutation, and treated the cells with MPA before fixation. To our expectation, wild-type zfIMPDH1a and wild-type zfIMPDH2 colocalized in all cytoophidia under MPA treatment. Yet, when there was either zfIMPDH1b ^{Y12A} or zfIMPDH2^{Y12A} present, cytoophidium assembly was completely inhibited (Supplementary Fig. 4), suggesting that all zfIMPDH isoforms interact within the cytoophidium. Altogether, our findings suggest that the zfIMPDH polymer and cytoophidium are structually similar to hIMPDHs.

2.3. zfIMPDH forms the cytoophidium in larvae

It has been demonstrated that the hIMPDH polymer structure enhances the resistance to allosteric inhibition from GTP binding, thereby promoting GTP production under physiological conditions (Johnson and Kollman, 2020). In our previous studies, we found the IMPDH cytoophidium in the spleen and pancreas of normal mouse (Chang et al., 2015; Keppeke et al., 2019). To examine whether zfIMPDH forms the cytoophidium in vivo, we performed whole-mount immunostaining on 8 days post fertilization (dpf) larvae (n = 10) with an anti-hIMPDH2 antibody; this antibody has been validated to target all three zfIMPDH isoforms (Figs. 2 and 3). In the eye and fin of larvae, we observed a few IMPDH cytoophidia in some specimens (Fig. 4A, B, K and L). Furthermore, in specific regions where bones are developing, many cytoophidia could be observed in all fish (Fig. 4C–J). Notably, at this larval stage, cartilage is the major component of the skeleton. Cytoophidia are also abundant in the Meckel's cartilage, operculum and pharyngeal teeth developing niches (Fig. 4C–J), suggesting that IMPDH cytoophidium formation is correlated with cartilage development and the dental stem cells. We also labeled IMPDH in embryos ranging from 2 to 12 hpf (hours post fertilization), in which we found no detectable cytoophidia (data not shown). The IMPDH inhibitor MPA can effectively induce IMPDH cytoophidium formation in vitro and in vivo in mammalian models (Keppeke et al., 2016). To further analyze how zfIMPDHs respond to MPA treatment in vivo, we treated 8 dpf larvae with MPA for 1 day. Consequently, a remarkable increase in the number and length of IMPDH cytoophidia were observed in cells of the olfactory organ in all treated larva (Fig. 5).

2.4. zfIMPDH forms the cytoophidium in adult fish

For further analysis of cytoophidium assembly in vivo, cryosections of adult fish (n = 4) were probed with the anti-IMPDH antibody. Tissues were identified based on published references (Menke et al., 2011). In the eye sections, abundant cytoophidia were observed in the outer nuclear layer and outer plexiform layer of the retina, where the photoreceptor cells are located (highlighted by yellow dashed lines in Fig. 6A–C). However, no cytoophidia were observed in the cornea (Fig. 6D). On the other hand, a group of cells in the interior of early differentiation teeth in the cap and bell stages display many cytoophidia (arrows in Fig. 6E–I). According to their localization, these cells are suspected to be dental stem cells. Meanwhile, the cytoophidium was not present in teeth in the late eruption phase (Fig. 6J).

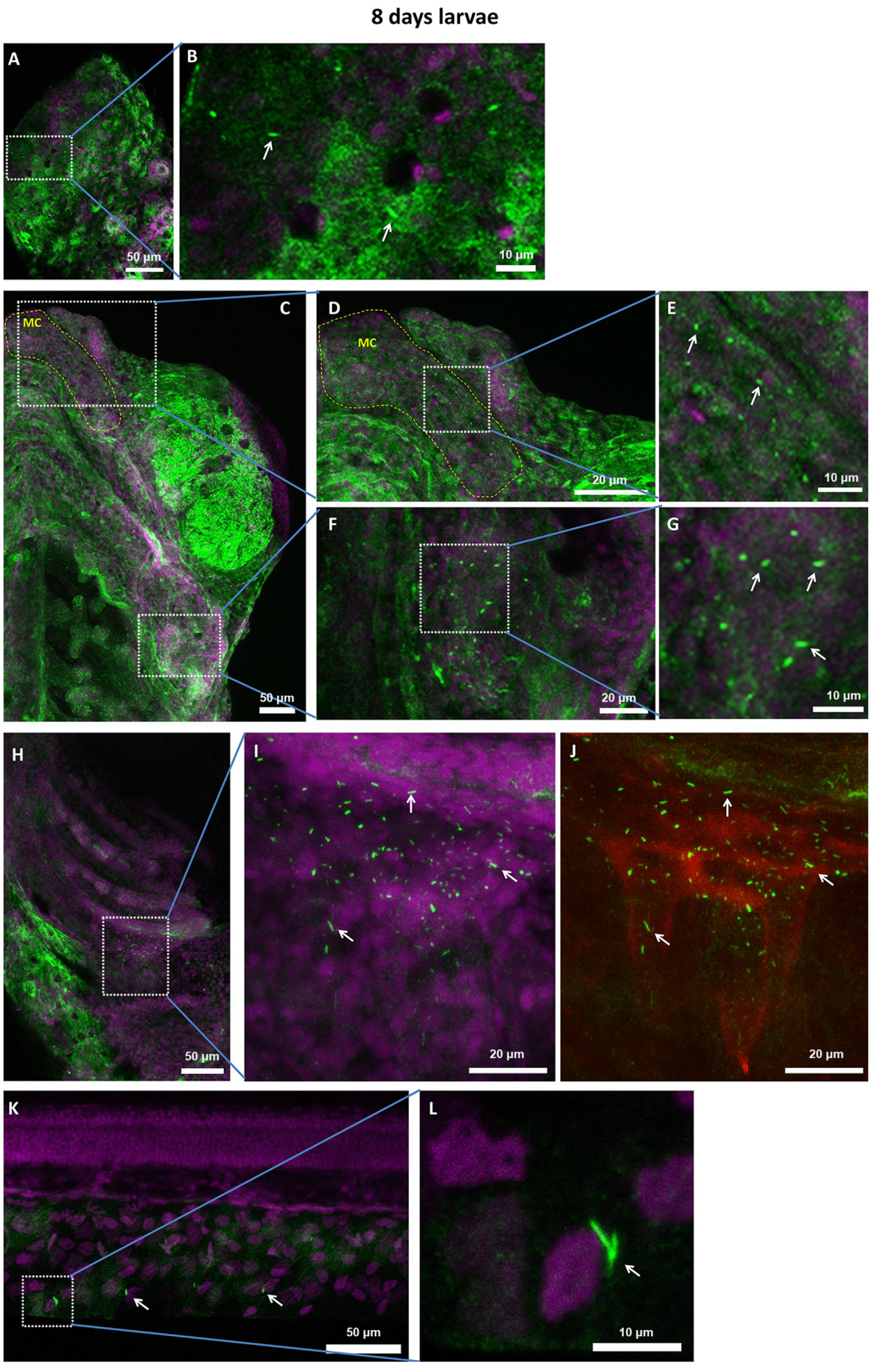

(caption on next page)

Fig. 4. IMPDH cytoophidia in 8 dpf zebrafish larvae. Whole-mount immunofluorescence of 8dpf larvae with anti-IMPDH2 antibody (shown in green) and DAPI (magenta). (A) Cytoophidia in the eye. (B) Zoom-in view of selected region in (A). (C) Ventral view of the head of larva. (D) Many cytoophidia were observed in the Meckel's cartilage (highlighted by yellow dashed lines in (C) and (D). (E) Zoom-in view of selected region in (D). (F) Cytoophidia were observed in the operculum. (G) Magnified image of selected region in (F). (H) Ventral view of ceratobranchials. (I and J) Zoom-in view of selected area in (H). The auto-fluorescence (red) shown in (J) reveals the contour of pharyngeal teeth, with abundant cytoophidia. (K and L) Some cells in the fin display cytoophidia. Arrows in all panels indicate cytoophidia. Scale bars = 50 μm in (A), (C), (H) and (K); 20 μm in (D), (F), (I) and (J); 10 μm in (B), (E), (G) and (L).

We also observed many cytoophidia in the pseudobranch and primary lamella of the gills in adult fish. In the pseudobranch, cytoophidia were distributed throughout the organ (arrows in Fig. 7A–D). In the gills, they were located in the structure providing cartilaginous support, in the primary lamella region, in which chondrocytes reside and produce the cartilaginous matrix (Fig. 7E–H). Interestingly, in most of the chondrocytes, cytoophidia were located in the nucleus (arrow in Fig. 7I).

Cytoophidia were also observed in the vitellogenic and pre-ovulatory follicles of the ovary (arrows in Fig. 8A–E). The cytoophidium was usually located in the thick *zona radiata* of the oocyte, which is surrounded by a layer of follicle cells (highlighted by yellow dashed lines in Fig. 8B). The *zona radiata* is present in stage 4 vitellogenic primary oocytes and pre-ovulatory follicles (Presslauer et al., 2014). We also screened the liver, intestine, cerebellum, olfactory organ, muscle and skin, where no cytoophidia were observed (Fig. 8F and Supplementary Fig. 5).

Quantificatative data show that cytoophidium was observed in ~80% of photoreceptor cells, and ~20–30% of cells in the teeth, pseudobranch, the gill's primary lamella and follicular cells of the ovary (Fig. 8F). Taken together, our findings demonstrate that zfIMPDH forms the cytoophidium in multiple tissues and at different developmental stages. Considering the advantages of using zebrafish as the research model, further studies on zebrafish cytoophidium would facilitate investigation into the physiological importance of IMPDH cytoophidia in vertebrates.

3. Discussion

In the last decade, intensive studies have been done to investigate the novel subcellular compartmentalization of metabolic enzymes - the cytoophidium. The IMPDH cytoophidium is proposed to enhance GTP production under physiological conditions, especially in proliferative cells (Johnson and Kollman, 2020; Keppeke et al., 2018). In mammalian models, formation of the IMPDH cytoophidium has been shown to correlate with rapid cell proliferation of pluripotent stem cells and antigen-activated lymphocytes (Calise et al., 2018; Duong-Ly et al., 2018;

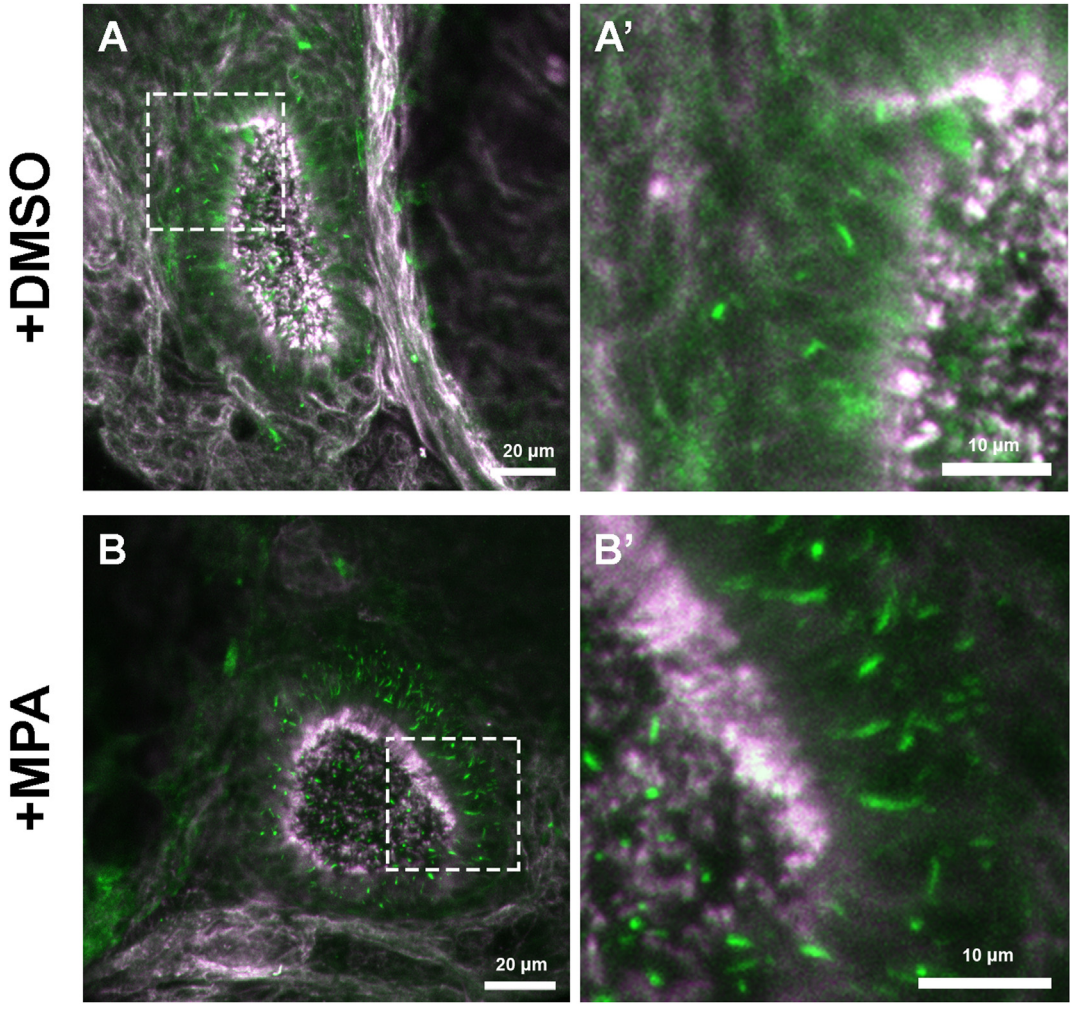

Fig. 5. MPA promotes IMPDH cytoophidium assembly in olfactory organ of larvae. Immunofluorescence images of the olfactory organ of 8 dpf larvae treated with 0.1% DMSO (A) or 100 μM MPA (B) for 1 day. (A′ and B′) Magnified images of selected areas in (A) and (B). IMPDH is shown in green and tubulin is shown in magenta. Scale bars = 20 μm in (A) and (B); 10 μm in (A′) and (B′).

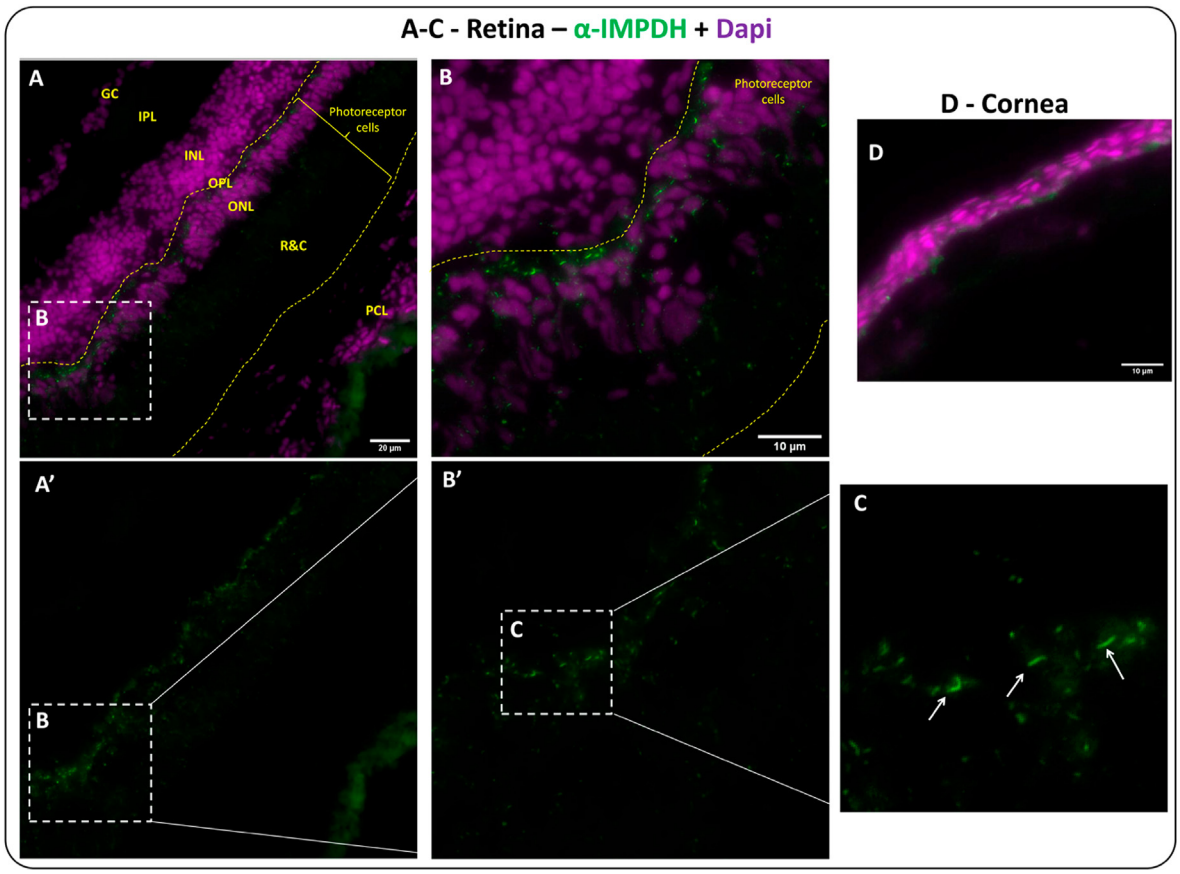

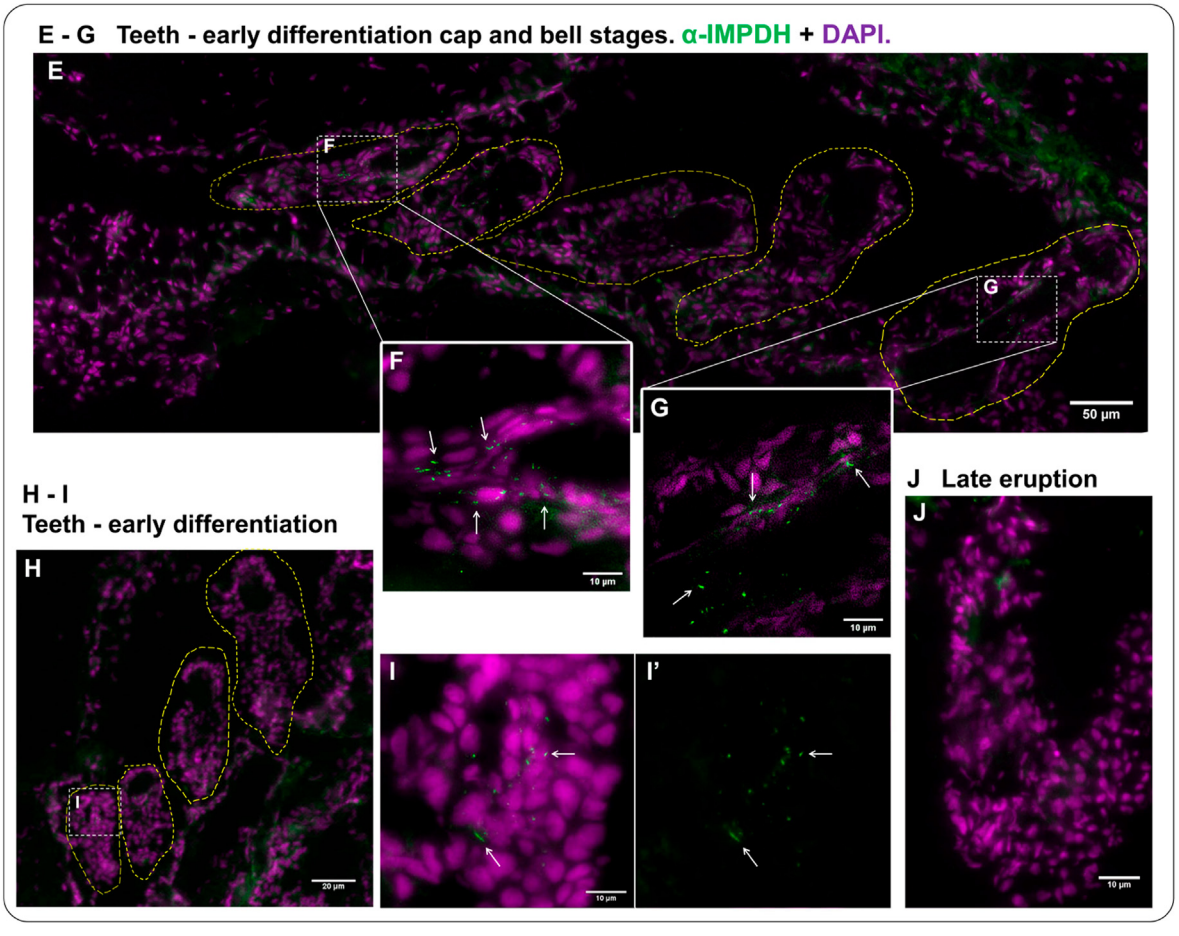

(caption on next page)

Fig. 6. IMPDH forms cytoophidia in the retina and teeth of adult fish. Immunofluorescence images of retina and teeth of adult zebrafish cryosections for IMPDH (green) and DAPI (magenta). (A–D) Abundant cytoophidia were observed in the outer nuclear layer and outer plexiform layer of the retina (arrows in C), and some were found in the rods and cones layer (A–C), but no cytoophidia were detected in the cornea (D). Highlighted by yellow dashed lines in (A″ and B″) is the region where photoreceptor cells are located. (B) Magnified image of selected region in (A). (C) Magnified image of selected region in (B). GC = ganglion cells, IPL = inner plexiform layer, INL = inner nuclear layer, OPL = outer plexiform layer, ONL = outer nuclear layer, R&C = rods and cones, PCL = pigment cell layer. (E–J) Cytoophidia were present in cells in the interior of teeth at early differentiation cap and bell stages (highlighted by yellow dashed lines in E and H), but not in the late eruption phase (J). (F and G) Magnified image of selected region in (E). (I) Magnified image of selected region in (H). Arrows in F, G and I indicate cytoophidia. Scale bars = 50 μm in (E); 20 μm in (A) and (H); 10 μm in (B), (D), (F), (G), (I) and (J).

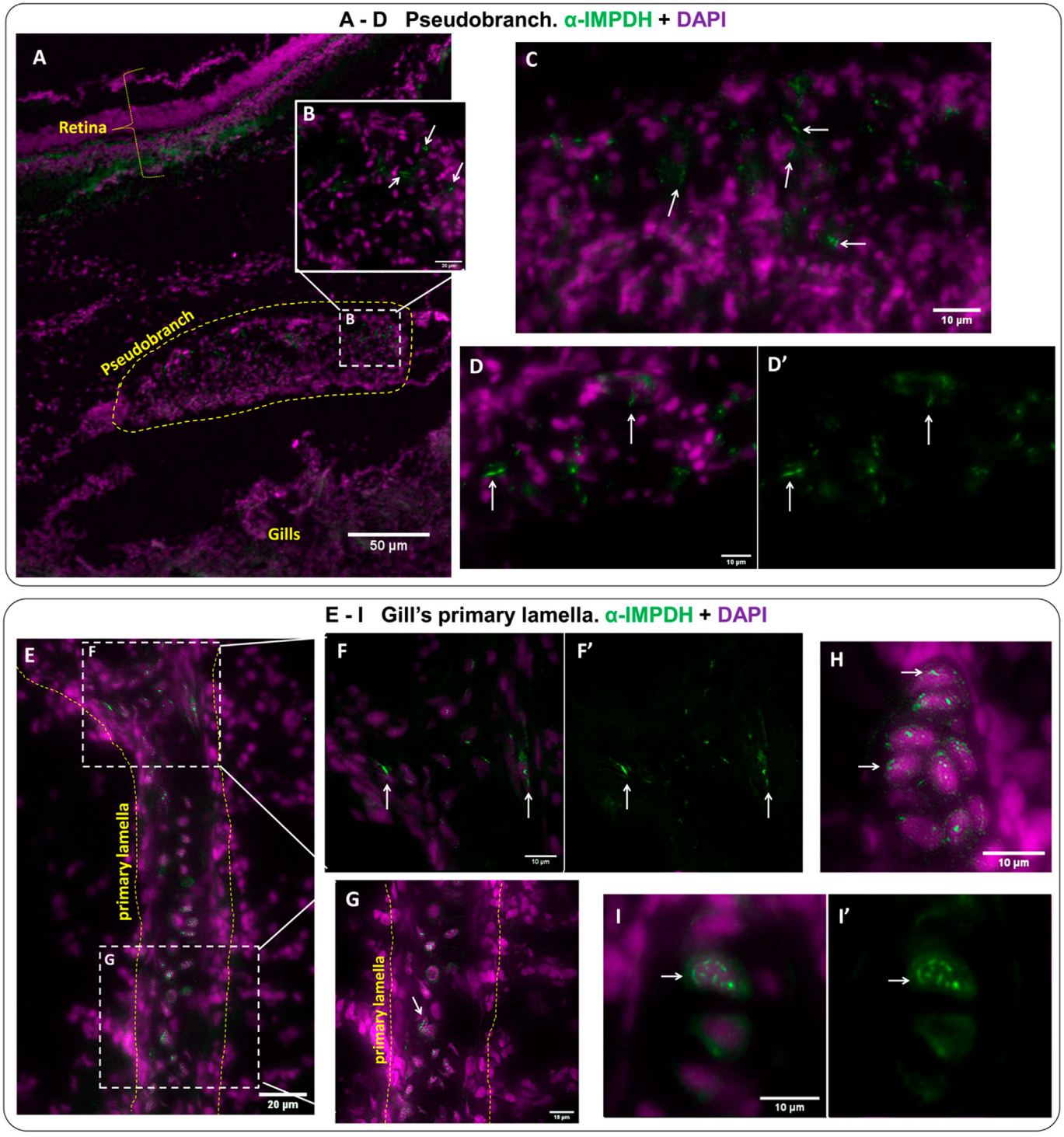

Fig. 7. IMPDH forms cytoophidia in pseudobranch and the primary lamella of the gill in adult fish. Immunofluorescence images of pseudobranch and gill of adult zebrafish cryosections for IMPDH (green) and DAPI (magenta). (A–D) Abundant cytoophidia were observed throughout the pseudobranch of the fish, highlighted in (A) by dashed lines. (B) Magnified image of selected region in (A). Arrows indicate cytoophidia in (B, C and D). (E–I) Cytoophidia were found in the primary lamella chondrocytes of the gill's cartilaginous support. In many cells cytoophidia were located in the nucleus (I). (F and G) Magnified images of selected regions in (E). Arrows indicate cytoophidia in (F–I). Scale bars = 50 μm in (A); 20 μm in (E); 10 μm in (B–D) and (F–I).

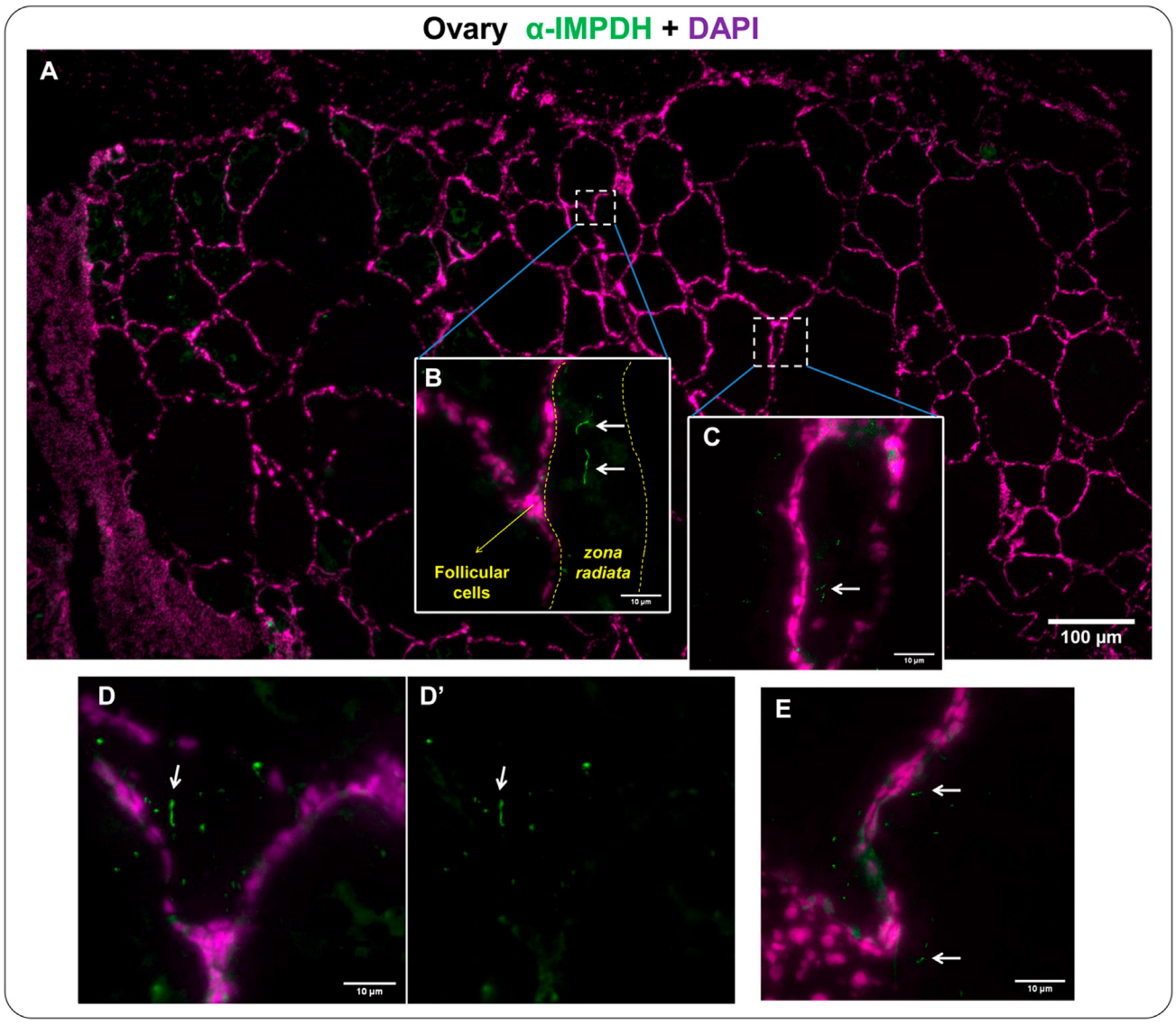

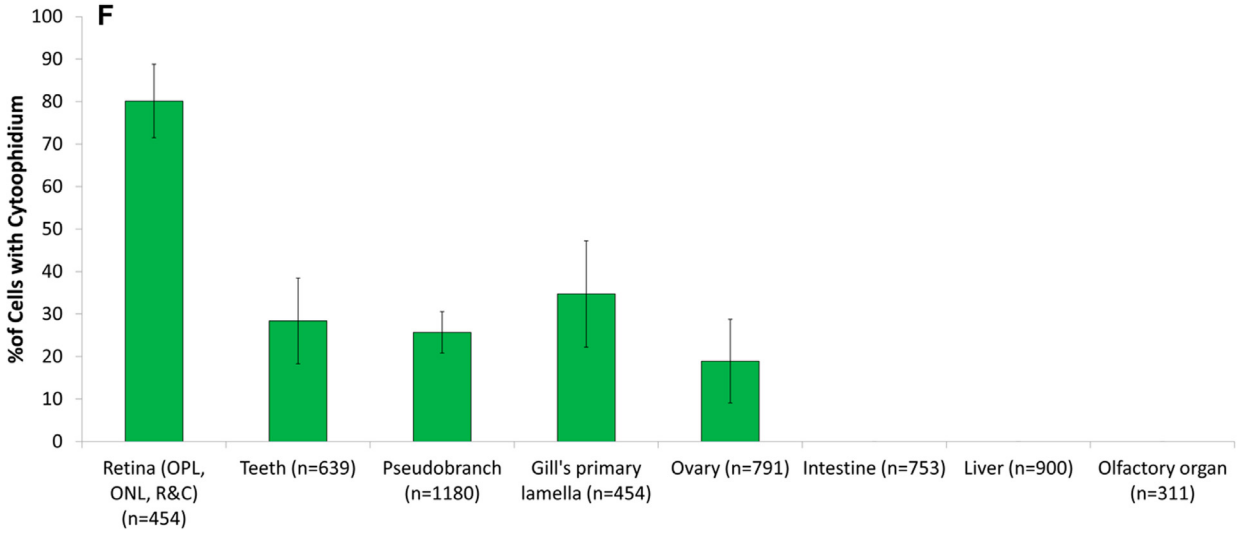

Fig. 8. IMPDH forms cytoophidia in the ovary of adult fish. Immunofluorescence images of the ovarian tissue of adult zebrafish cryosections for IMPDH (green) and DAPI (magenta). (A–E) Cytoophidia were observed in the vitellogenic and pre-ovulatory follicles. Cytoophidia were frequently located in the thick *zona radiata* of oocytes (B). Arrows indicate the cytoophidia in (B–E). Scale bars = 100 µm in (A); 10 µm in (B–E). (F) Quantification of cells presenting cytoophidia in the different tissues of adult fish. (n) indicate the number of cells counted. Error bars = S.D.

Keppeke et al., 2018). In other tissues, the presence of the IMPDH cytoophidium might be associated with the insulin-secretory signals in mouse beta cells and the light response of photoreceptor cells in mouse retina, suggesting the association between this structure and multiple physiological events (Chang et al., 2015; Plana-Bonamaiso et al., 2020).

In this study, we demonstrate that the cytoophidium-forming properties of zebrafish IMPDH isoforms.IMPDH cytoophidium is likely conserved among vertebrate species and may have originated much earlier during the evolution. The cytoophidium-forming tendency of zfIMPDH1a is particularly intriguing. When it is expressed in HeLa cells, zfIMPDH1a rarely forms cytoophidia under induction. However, in HEp-2 cells zfIMPDH1a cytoophidia or clumps could be observed in many cells under the treatments of DON or MPA, suggesting the regulation of zfIMPDH1a in forming the cytoophidium could be variable in different cell types. Indeed, zfIMPDH1a is mainly expressed in the eye, where many cytoophidia could be observed. IMPDH cytoophidia in the fish retina are distributed largely in the outer layer region, where photoreceptor cells are located. These data corroborate a recently study showing that IMPDH aggregate formation in mouse photoreceptor cells correlates with bright light exposure and increased production of GTP and ATP (Plana-Bonamaiso et al., 2020). We therefore hypothesize that the function of the IMPDH cytoophidium in retinal cells, which is likely associated with the intense guanosine nucleotide production required to support the phototransduction process, is conserved among vertebrates.

We also show that cytoophidia are present in a specific cell population in the interior of early differentiation teeth. Further analysis is required to determine whether the IMPDH cytoophidium could be a marker for dental stem cells and its function in correlation with dental development. Moreover, IMPDH cytoophidia are displayed by chondrocytes at various regions in larval and adult fish, such as Meckel's cartilage, operculum, pharyngeal teeth and the pseudobranch. In most of the gill's primary lamella chondrocytes, cytoophidia were found in the nucleus. Although nuclear cytoophidia are frequently seen in cultured cells, the functional differences between nuclear and cytoplasmic cytoophidia are largely unknown (Gou et al., 2014; Juda et al., 2014). Our results indicate that the nuclear cytoophidium is also a natural phenomenon in vivo. Further study is needed to understand whether and how IMPDH cytoophidia participate in the specific metabolism of chondrocytes.

Zebrafish have been used in biological study since the 1930's. One of many reasons for this species' popularity in genetic research is the convenience of generating transgenic individuals. Since a great number of molecular tools for genome editing have been established in the last few years, the generation of mutant vertebrate models for cytoophidium research could be accelerated. We have shown that the point mutation Y12A, which disrupt IMPDH polymerization or cytoophidium assembly in mammalian IMPDHs also prevent zfIMPDH cytoophidium formation. Future works applying these mutations to the zebrafish experimental model would greatly benefit the investigation into the physiological importance of the IMPDH cytoophidium.

4. Methods

4.1. Animals

Zebrafish (*Danio rerio*) AB strain was used throughout this study. Embryos and fish were kept at 28.5 °C for all subsequent assays. In total, 4 adult fish were used for RNA collection and 4 adult fish were used for cryosections. Maintenance and sacrifice of the animals were performed following ethics recommendations. Animals were euthanized by rapid chilling (2°–4 °C) for at least 10 min, as recommended by the AVMA Guidelines for the Euthanasia of Animals (Leary et al., 2020).

4.2. Constructs

Zebrafish IMPDH coding sequences for the isoforms 1a, 1b and 2 (NCBI Reference Sequence: NM_001002177.1; NM_001014369.2; NM_201464.1) were amplified with primers shown in Supplementary Table 1 from zebrafish cDNA (see RT-qPCR methods for details) and inserted into the linearized pCMV3 vector (Sino Biological) with tags at the N-terminus (Myc for zfIMPDH1a, HA for zfIMPDH1b and Flag for zfIMPDH2) by using ClonExpress UItra One Step Cloning Kit (C115, Vazyme) according to the manufacturer's protocol. Site-directed mutagenesis was carried out by linearizing target constructs with primers containing individual point mutations (Supplementary Table 1), followed by recirculation of the plasmid with ClonExpress One Step Cloning Kit (C113, Vazyme).

4.3. Cell culture and transfection

HeLa cells (93021013, Public Health England) and HEp-2 cells (CCL-23, ATCC) were cultured in DMEM with high glucose (Thermo Fisher Scientific) and supplemented with 10% FBS (Thermo Fisher Scientific), 2 mM L-Glutamine and 1% Gibco Antibiotic-Antimycotic (Thermo Fisher Scientific). All cells were cultured in a 37 °C humid incubator with 5% CO_2. For cell transfection, TurboFect or Lipofectamine 3000 transfection reagent (R0531 or L3000001, Thermo Fisher Scientific) was used according to instructions provided by the manufacturer. MPA (Mycophenolic acid, J61905, Alfa Aesar) was dissolved in DMSO (Sigma-Aldrich) and added to the culture medium at 100 μM final concentration. DON (6-diazo-5-oxo-L-norleucine, D2141, Sigma-Aldrich) was solubilized in water to a 100 mM stock solution and added to the culture medium at a final concentration of 100 μM.

4.4. Immunofluorescence in cultured cells, whole-mounted larvae and adult cryosections

Immunofluorescence probing on cultured cells was performed as previously described (Keppeke et al., 2015). Whole-mounted larvae immunofluorescence, including fixation, de/rehydration, permeabilization and antibody probing, was performed following the published protocol (Santos et al., 2018). For the adult zebrafish, specimens were sacrificed and the entire animal was immediately embedded with Tissue-Tek O.C.T. compound (Sakura) and stored at −80 °C. Cryosections were cut to 5 μm thick in a lateral view. Sections were then fixed with 4% paraformaldehyde for 20 min, followed by blocking with Background Sniper (BS966, Biocare) for 15 min. After washing with PBS, sections were then incubated overnight at 4 °C with primary antibody at 1:300 dilution with staining buffer (PBS supplemented with 0.5% Tween and 1% BSA). After washing three times with PBS, sections were incubated for 2 h at room temperature with secondary antibody 1:500 dilution in staining buffer with DAPI. After washing three times with PBS, sections were mounted and observed under a fluorescent microscope. Organs and tissues on cryosections were identified by comparing nuclear staining and tissue morphology with published references (Menke et al., 2011).

Antibodies used in this study: rabbit polyclonal anti-IMPDH2 antibody (12948-1-AP, ProteinTech), mouse anti-Myc monoclonal antibody 9E10 (sc-40, Santa Cruz Biotech), mouse anti-HA antibody (sc-7392, Santa Cruz Biotech), mouse anti-HA monoclonal antibody HA-7 (H3663, Sigma-Aldrich), mouse anti-Flag M2 antibody (F1804, Sigma-Aldrich), mouse anti-tubulin antibody (MAB1637, Sigma-Aldrich), rabbit polyclonal anti-DYKDDDDK-tag Flag antibody (MBS821829, MyBioSource). DyLight 488-conjugated, Cy™3-conjugated and DyLight 649-conjugated donkey polyclonal anti-mouse IgG antibody (715-165-151, 715-485-151, 715-495-151, Jackson ImmunoResearch), Cy™3-conjugated donkey polyclonal anti-rabbit IgG antibody (711-165-152, Jackson ImmunoResearch), Alexa Fluor® 488-conjugated, Alexa Fluor® 647-conjugated donkey polyclonal anti-rabbit IgG antibody (A-21206, A-31573, Invitrogen Mol Probes).

4.5. Immunoblotting

Cells were lysed in RIPA lysis buffer (20–188, Millipore) and 10 μg

total protein was run for each lane on a 12% polyacrylamide gel. The PVDF membrane with 0.45 μm pole size (GE Healthcare) was used for protein transfer. The membrane was incubated with 5% milk in PBS at room temperature for 1 h for blocking, followed by overnight incubation with primary antibodies at 4 °C. Primary antibody was washed away from the membrane with PBST for three times. Further incubation with secondary antibodies was perform at 4 °C for overnight. After three times washing with PBST, the signals were detected using ECL (WBLUF0500, Millipore) and the GeneGnoe XRQ chemiluminescence imaging system (Syngene). Antibodies used for immunoblotting include: mouse anti-HA IgG (1:3000, sc-7392, Santa Cruz), mouse anti-Flag IgG (1:3000, F3165, Sigma-Aldrich), mouse anti-myc (1:1000, sc-40, Santa Cruz).

4.6. RT-qPCR

Adult zebrafish were sacrificed and eye, muscle, intestine, and a mix of organs were collected immediately. The mix of organs contained parts of liver, kidney, pancreas, heart, gills, spleen and perhaps other organs. For the 10 dpf larvae, the entire animal was used. Samples were ground up with a tissue homogenizer and RNA was extracted using TransZol Up Plus RNA Kit (ER501, TransGen Biotech). Reverse transcription was performed with PrimeScrip RT Master Mix (RR036A, Takara). Quantitative PCR (qPCR) was performed with ChamQ Universal SYBR qPCR Master Mix (Q711-02, Vazyme), and the signal was detected by the QuantStudio 7 Flex System (Applied Biosystems), following manufacturer's protocol. Standard 60° Tm annealing temperature and 40 amplification cycles were used for all primer pairs. The quality of reaction was evaluated by melt curves. Target Ct genes were analyzed by comparison of housekeeping references through the ΔΔCt method (Livak and Schmittgen, 2001). First delta was housekeeping geomean. Second delta was larval levels. Housekeeping was a geomean of β-Act, GAPDH, HPRT1 and TUBα-1a. Primers targeting specific zfIMPDH isoforms for RT-qPCR were referred from a previous study (Li et al., 2015). All primer sequences are presented in Supplementary Table 1.

4.7. Microscope and image analysis

Fluorescent images were acquired with a laser-scanning confocal microscope (TCS SP8 STED 3X, Leica) and the fluorescent microscope Axio Imager Z2 or M2 (Zeiss) under 20X and 40X objectives. Images were analyzed with ImageJ software.

4.8. Statistics

Quantifications were performed on captured images from at least two in vitro experimental replicates, or the adult specimens enrolled in the study. Averages and standard deviation (S.D.) or standard error of the mean (S.E.M.) is shown. The number of cells counted is indicated in each experiment. Average Ct values in the RT-qPCR analysis and the average of cells presenting cytoophidium or clumps were statistically compared by the *t*-test with Welch's correction. *P*-value <0.05 was considered statistically significant. Statistical analysis was performed with GraphPad Prism software.

Funding

This work was supported by ShanghaiTech University and FAPESP (Fundação de Amparo à Pesquisa do Estado de São Paulo) grant number #2017/20745-1. Funding providers had no involvement in the study design, collection, analysis and interpretation of data, writing of the report, and in the decision to submit the article for publication.

Declaration of competing interest

The authors declare no conflicts of interest.

Appendix A. Supplementary data

Supplementary data to this article can be found online at https://doi.org/10.1016/j.ydbio.2021.05.017.

References

Anthony, S.A., Burrell, A.L., Johnson, M.C., Duong-Ly, K.C., Kuo, Y.M., Simonet, J.C., Michener, P., Andrews, A., Kollman, J.M., Peterson, J.R., 2017. Reconstituted IMPDH polymers accommodate both catalytically active and inactive conformations. Mol. Biol. Cell. 28 (20), 2600–2608.

Buey, R.M., Ledesma-Amaro, R., Velazquez-Campoy, A., Balsera, M., Chagoyen, M., de Pereda, J.M., Revuelta, J.L., 2015. Guanine nucleotide binding to the Bateman domain mediates the allosteric inhibition of eukaryotic IMP dehydrogenases. Nat. Commun. 6, 8923.

Calise, S.J., Abboud, G., Kasahara, H., Morel, L., Chan, E.K.L., 2018. Immune response-dependent assembly of IMP dehydrogenase filaments. Front. Immunol. 9, 2789.

Calise, S.J., Carcamo, W.C., Krueger, C., Yin, J.D., Purich, D.L., Chan, E.K., 2014. Glutamine deprivation initiates reversible assembly of mammalian rods and rings. Cell. Mol. Life Sci. : CMLS. 71 (15), 2963–2973.

Calise, S.J., Purich, D.L., Nguyen, T., Saleem, D.A., Krueger, C., Yin, J.D., Chan, E.K., 2016. 'Rod and ring' formation from IMP dehydrogenase is regulated through the one-carbon metabolic pathway. J. Cell Sci. 129 (15), 3042–3052.

Carcamo, W.C., Satoh, M., Kasahara, H., Terada, N., Hamazaki, T., Chan, J.Y., Yao, B., Tamayo, S., Covini, G., von Muhlen, C.A., Chan, E.K., 2011. Induction of cytoplasmic rods and rings structures by inhibition of the CTP and GTP synthetic pathway in mammalian cells. PloS One. 6 (12), e29690.

Carr, S.F., Papp, E., Wu, J.C., Natsumeda, Y., 1993. Characterization of human type I and type II IMP dehydrogenases. J. Biol. Chem. 268 (36), 27286–27290.

Chang, C.C., Keppeke, G.D., Sung, L.Y., Liu, J.L., 2018. Interfilament interaction between IMPDH and CTPS cytoophidia. FEBS J. 285 (20), 3753–3768.

Chang, C.C., Lin, W.C., Pai, L.M., Lee, H.S., Wu, S.C., Ding, S.T., Liu, J.L., Sung, L.Y., 2015. Cytoophidium assembly reflects upregulation of IMPDH activity. J. Cell Sci. 128 (19), 3550–3555.

Duong-Ly, K.C., Kuo, Y.M., Johnson, M.C., Cote, J.M., Kollman, J.M., Soboloff, J., Rall, G.F., Andrews, A.J., Peterson, J.R., 2018. T cell activation triggers reversible inosine-5'-monophosphate dehydrogenase assembly. J. Cell Sci. 131 (17), jcs223289.

Fernandez-Justel, D., Nunez, R., Martin-Benito, J., Jimeno, D., Gonzalez-Lopez, A., Soriano, E.M., Revuelta, J.L., Buey, R.M., 2019. A nucleotide-dependent conformational switch controls the polymerization of human IMP dehydrogenases to modulate their catalytic activity. J. Mol. Biol. 431 (5), 956–969.

Gou, K.M., Chang, C.C., Shen, Q.J., Sung, L.Y., Liu, J.L., 2014. CTP synthase forms cytoophidia in the cytoplasm and nucleus. Exp. Cell Res. 323 (1), 242–253.

Hager, P.W., Collart, F.R., Huberman, E., Mitchell, B.S., 1995. Recombinant human inosine monophosphate dehydrogenase type I and type II proteins. Purification and characterization of inhibitor binding. Biochem. Pharmacol. 49 (9), 1323–1329.

Hedstrom, L., 2009. IMP dehydrogenase: structure, mechanism, and inhibition. Chem. Rev. 109 (7), 2903–2928.

Ji, Y., Gu, J., Makhov, A.M., Griffith, J.D., Mitchell, B.S., 2006. Regulation of the interaction of inosine monophosphate dehydrogenase with mycophenolic Acid by GTP. J. Biol. Chem. 281 (1), 206–212.

Johnson, M.C., Kollman, J.M., 2020. Cryo-EM structures demonstrate human IMPDH2 filament assembly tunes allosteric regulation. eLife 9, e53243.

Juda, P., Smigova, J., Kovacik, L., Bartova, E., Raska, I., 2014. Ultrastructure of cytoplasmic and nuclear inosine-5'-monophosphate dehydrogenase 2 "rods and rings" inclusions. J. Histochem. Cytochem. 62 (10), 739–750.

Keppeke, G.D., Barcelos, D., Fernandes, M., Comodo, A.N., Guimaraes, D.P., Cardili, L., Carapeto, F.C.L., Andrade, L.E.C., Landman, G., 2020. IMP dehydrogenase rod/ring structures in acral melanomas. Pigm. Cell Melanoma Res. 33 (3), 490–497.

Keppeke, G.D., Calise, S.J., Chan, E.K., Andrade, L.E., 2015. Assembly of IMPDH2-based, CTPS-based, and mixed rod/ring structures is dependent on cell type and conditions of induction. J. Genet. Genomics. 42 (6), 287–299.

Keppeke, G.D., Calise, S.J., Chan, E.K.L., Andrade, L.E.C., 2019. Ribavirin induces widespread accumulation of IMP dehydrogenase into rods/rings structures in multiple major mouse organs. Antivir. Res. 162, 130–135.

Keppeke, G.D., Chang, C.C., Peng, M., Chen, L.Y., Lin, W.C., Pai, L.M., Andrade, L.E.C., Sung, L.Y., Liu, J.L., 2018. IMP/GTP balance modulates cytoophidium assembly and IMPDH activity. Cell Div. 13, 5.

Keppeke, G.D., Prado, M.S., Nunes, E., Perazzio, S.F., Rodrigues, S.H., Ferraz, M.L., Chan, E.K., Andrade, L.E., 2016. Differential capacity of therapeutic drugs to induce Rods/Rings structures in vitro and in vivo and generation of anti-Rods/Rings autoantibodies. Clin. Immunol. 173, 149–156.

Leary, S., Underwood, W., Anthony, R., Cartner, S., Grandin, T., Greenacre, C., Gwaltney-Brant, S., McCrackin, M.A., Meyer, R., Miller, D., Shearer, J., Turner, T., Yanong, R., 2020. AVMA Guidelines for the Euthanasia of Animals: 2020 Edition. AVMA, Schaumburg, IL, USA.

Li, Y., Li, G., Gorling, B., Luy, B., Du, J., Yan, J., 2015. Integrative analysis of circadian transcriptome and metabolic network reveals the role of de novo purine synthesis in circadian control of cell cycle. PLoS Comput. Biol. 11 (2), e1004086.

Lin, W.C., Chakraborty, A., Huang, S.C., Wang, P.Y., Hsieh, Y.J., Chien, K.Y., Lee, Y.H., Chang, C.C., Tang, H.Y., Lin, Y.T., Tung, C.S., Luo, J.D., Chen, T.W., Lin, T.Y., Cheng, M.L., Chen, Y.T., Yeh, C.T., Liu, J.L., Sung, L.Y., Shiao, M.S., Yu, J.S., Chang, Y.S., Pai, L.M., 2018. Histidine-dependent protein methylation is required for compartmentalization of CTP synthase. Cell Rep. 24 (10), 2733–2745.

Liu, J.L., 2010. Intracellular compartmentation of CTP synthase in Drosophila. J. Genet. Genomics. 37 (5), 281–296.
Liu, J.L., 2016. The cytoophidium and its kind: filamentation and compartmentation of metabolic enzymes. Annu. Rev. Cell Dev. Biol. 32, 349–372.
Livak, K.J., Schmittgen, T.D., 2001. Analysis of relative gene expression data using real-time quantitative PCR and the 2(-Delta Delta C(T)) Method. Methods 25 (4), 402–408.
Lynch, E.M., Kollman, J.M., Webb, B.A., 2020. Filament formation by metabolic enzymes-A new twist on regulation. Curr. Opin. Cell Biol. 66, 28–33.
Menke, A.L., Spitsbergen, J.M., Wolterbeek, A.P., Woutersen, R.A., 2011. Normal anatomy and histology of the adult zebrafish. Toxicol. Pathol. 39 (5), 759–775.
Naffouje, R., Grover, P., Yu, H., Sendilnathan, A., Wolfe, K., Majd, N., Smith, E.P., Takeuchi, K., Senda, T., Kofuji, S., Sasaki, A.T., 2019. Anti-tumor potential of IMP dehydrogenase inhibitors: a century-long story. Cancers (Basel). 11 (9), 1346.
Noree, C., Begovich, K., Samilo, D., Broyer, R., Monfort, E., Wilhelm, J.E., 2019. A quantitative screen for metabolic enzyme structures reveals patterns of assembly across the yeast metabolic network. Mol. Biol. Cell 30 (21), 2721–2736.
Peng, Min, Chang, Chia-Chun, Liu, Ji-Long, Sung, Li-Ying, 2021. CTPS and IMPDH form cytoophidia in developmental thymocytes. Exp. Cell Res. 405 (1) https://doi.org/10.1016/j.yexcr.2021.112662. Online ahead of print.
Plana-Bonamaiso, A., Lopez-Begines, S., Fernandez-Justel, D., Junza, A., Soler-Tapia, A., Andilla, J., Loza-Alvarez, P., Rosa, J.L., Miralles, E., Casals, I., Yanes, O., de la Villa, P., Buey, R.M., Mendez, A., 2020. Post-translational regulation of retinal IMPDH1 in vivo to adjust GTP synthesis to illumination conditions. eLife 9, e56418.
Presslauer, C., Nagasawa, K., Dahle, D., Babiak, J., Fernandes, J.M., Babiak, I., 2014. Induced autoimmunity against gonadal proteins affects gonadal development in juvenile zebrafish. PloS One 9 (12), e114209.
Ruan, H., Song, Z., Cao, Q., Ni, D., Xu, T., Wang, K., Bao, L., Tong, J., Xiao, H., Xiao, W., Cheng, G., Xiong, Z., Liang, H., Liu, D., Wang, L., Olivier, T., Jane, B.H., Yang, H., Zhang, X., Chen, K., 2020. IMPDH1/YB-1 positive feedback loop assembles cytoophidia and represents a therapeutic target in metastatic tumors. Mol. Ther. 28 (5), 1299–1313.
Santos, D., Monteiro, S.M., Luzio, A., 2018. General whole-mount immunohistochemistry of zebrafish (Danio rerio) embryos and larvae protocol. Methods Mol. Biol. 1797, 365–371.
Senda, M., Natsumeda, Y., 1994. Tissue-differential expression of two distinct genes for human IMP dehydrogenase (E.C.1.1.1.205). Life Sci. 54 (24), 1917–1926.
Shen, Q.J., Kassim, H., Huang, Y., Li, H., Zhang, J., Li, G., Wang, P.Y., Yan, J., Ye, F., Liu, J.L., 2016. Filamentation of metabolic enzymes in Saccharomyces cerevisiae. J. Genet. Genomics. 43 (6), 393–404.